RSC Advances

ROYAL SOCIETY OF CHEMISTRY

www.rsc.org/advances

RSC Advances

ARTICLE

Microwave-assisted in-situ synthesis of reduced graphene oxide/Mn_3O_4 composites for supercapacitor application

Received 00th January 20xx,
Accepted 00th January 20xx

DOI: 10.1039/x0xx00000x

www.rsc.org/

Haiyan Zhang*, Zidong Huang, Yunyong Li*, Yiming Chen, Wenguang Wang, Yipeng Ye, Peng Deng

Reduced graphene oxide/Mn_3O_4 (GM) composites were prepared by a simple and convenience strategy, that is, microwave irradiation of the hydrothermal product of reduced graphene oxide-$Mn(NO_3)_2$ mixtures. Mn_3O_4 nanoparticles with size of 20-50 nm were uniformly distributed on the surface of reduced graphene oxides. The GM composites exhibited good electrochemical performance with a specific capacitance of 344.8 F g^{-1} at the discharge current density of 1 A g^{-1} using 5 M NaOH as electrolytes. The energy density of GM composites was as high as 47.8 Wh kg^{-1} with the power density of 1000 W kg^{-1}. After 5000 cycles of charge/discharge experiments, a high level retaining specific capacitance of 342.1 F g^{-1} was obtained with 99.2% retention of the initial capacitance at 1 A g^{-1} and the equivalent series resistance of the GM composites system was much lower than that of pure Mn_3O_4. Therefore, the GM composites with large capacitance, good cycling performance and reversibility can be used as a promising electrode material for supercapacitor application.

1. Introduction

Supercapacitors have drawn tremendous attention in the field of electronic devices and electric vehicles owing to their higher power densities compared with secondary batteries and higher energy densities than electrostatic and electrolytic capacitors[1-4]. Supercapacitors can charge and discharge instantaneously，so they usually work as electric vehicle power unit to instantaneously provide large current for electric vehicles, which can improve the ability of acceleration and climbing of the electric vehicles. At the same time, they can reduce the damage from the large discharge current for power battery and extend the cycle life of the battery. So many countries have invested a lot of manpower, materials and financial resources to study supercapacitors. There are two kinds of supercapacitors involving electric double-layer capacitors (EDLCs) and pseudocapacitors depending on the charge conversion/storage mechanism. The electrostatic forces in the electrical double layers formed at the interface between electrode and electrolyte play an important role in the energy storage of EDLCs[5]. Generally, carbon materials, such as activated carbon, carbon nanotubes, and graphene, possesses large surface area and readily accessible mesopores, which have been widely used as electrode materials in EDLCs. Meanwhile, the charge storage mechanism of pseudocapacitors results from the fast Faradaic redox reaction between the electrolyte and electrode[6]. The electrode materials of pseudocapacitors generally involve various metal oxides and conductive polymers. However, EDLCs have high power density but suffer from low energy density, while pseudocapacitors possess a high specific capacitance but encounter poor cycle performance. Therefore, the combination of carbon materials and pseudo-capacitive materials is supposed to achieve the supercapacitors with high energy density and excellent cycling stability.

In recent years, transitions metal oxides have been extensively studied as pseudo-capacitive materials due to their higher capacitance than carbon materials and better cycling stability than conductive polymers[7-11]. Among various transition metal oxides, Mn_3O_4 is a potentially interesting material for supercapacitors due to its low cost, environmental benignity and relatively broad work potential window in aqueous solution[12-14]. However, the poor electronic conductivity (10^{-5}-10^{-6} S cm^{-1})[15] and cycling stability of Mn_3O_4 limit its further application for supercapacitors. Graphene, a flat monolayer of carbon atoms that tightly pack into a two-dimensional honeycomb lattice, has emerged as a promising material for supercapacitor application owing to its excellent electronic properties, such as high carrier mobility (200000 cm^2 V^{-1} S^{-1})[16], high thermal conductivity (5300 W m^{-1} K^{-1})[17] and large theoretical specific surface area (2600 m^2 g^{-1})[18]. Graphene/Mn_3O_4 composites have been widely used as a kind of electrode material for high-performance supercapacitors since graphene nanosheets can serve as a highly conductive matrix for anchoring metal oxide naopaticles[19]. Wang et al.[19] synthesized graphene/Mn_3O_4 nanocomposites by mixing graphene suspension in ethylene glycol with MnO_2 organosol, followed by subsequent ultrasonication processing and heat treatment. The specific capacitance of supercapacitors using graphene/Mn_3O_4 nanocomposites as electrode materials is up to

*Guangdong Provincial Key Laboratory of Functional Soft Condensed Matter, School of Material and Energy, Guangdong University of Technology, Guangzhou, 510006, China. *Corresponding author: Tel.: +86 2039322570; Fax: +86 2039322570. E-mail address: hyzhang@gdut.edu.cn (H.Y. Zhang), yunyong207@163.com (Y.Y. Li).*

175 F g^{-1} in 1 M Na_2SO_4 aqueous solution and 256 F g^{-1} in 6 M KOH aqueous solution, respectively. Lee et al.[20] prepared graphene/Mn_3O_4 nanorods composites by a simple hydrothermal process from $KMnO_4$ using ethylene glycol as reducing agent. The specific capacitance of the graphene/Mn_3O_4 nanorods composites was 121, 115, 107, 97, 88, 85 and 83 F g^{-1} at current density of 0.5, 1, 2, 5, 10, 15 and 20 A g^{-1}, repecetively. Zhang et al.[21]synthesized nanocomposites with Mn_3O_4 nanoparticles anchored on the graphene nanosheets by one-step solvothermal process, and the resulted graphene/ Mn_3O_4 nanocomposites exhibited a specific capacitance of 147 F g^{-1} and the capacitance loss of 5% after 500 consecutive cycles in 1 M Na_2SO_4 aqueous solution at a current density of 0.1 A g^{-1}. Wu et al.[22]prepared graphene/Mn_3O_4 composites via a simple solvothermal process by mixing $Mn(AC)_2{\cdot}4H_2O$ with graphite oxide suspension in ethanol-H_2O mixture. Under a potential window of -0.2 to 0.8 V, the composites delivered an initial specific capacitance of 161 F g^{-1} at 1 A g^{-1} and increased to 230 F g^{-1} after 1000 cycles.

In this paper, we prepared reduced graphene oxide/Mn_3O_4 (GM) composites via a simple and convenience strategy, that is, microwave-assisted in-situ synthesis of Mn_3O_4 nanoparticles on the graphene sheets. Reduced graphene oxides (RGO) were obtained by microwave radiation of graphite oxide (GO). GM composites were prepared by hydrothermal synthesis of aqueous mixture of RGO and $Mn(NO_3)_2$, followed by microwave irradiation of the hydrothermal synthesis product. Compared with the solvothermal methods, which need a long time to heat or dry the hydrothermal product to obtain Mn_3O_4/grphene composites, our strategy is more efficient and energy-saving. Additionally, the most important point to be noted is that, compared with the conventional microwave hydrothermal method which need in a condition of strong alkali or hydrazine hydrate (toxic), our strategy is green and environmentally friendly. The supercapacitors based on the as-prepared GM composites showed a far higher specific capacitance than RGO and more excellent cycling stability than pure Mn_3O_4.

2. Experimental

2.1 Preparation of RGO

Graphite oxide was prepared by a modified Hummers method[23]. Reduced graphene oxide was obtained by microwave radiation of GO in a microwave oven at 1000 W for 2 min in ambient condition and a large volume expansion was observed.

2.2 Preparation of GM composites

RGO was dispersed into distilled water under ultrasonic condition to form aqueous suspension with a concentration of 0.1 g L^{-1}. Then 100 mL of as-obtained RGO aqueous suspension was mixed with a $Mn(NO_3)_2$ aqueous solution. The mixture was transferred into an autoclave and heated at 180 ^oC for 24 h. After cooling down to room temperature, the intermediate product was collected and dried at 30 ^oC. Finally, the GM composites were obtained through microwave radiation at 1000 W for 2 min in ambient condition once again.

2.3 Characterization of samples

X-ray diffraction spectroscopy (XRD; DMAX-Ultima IV, Rigaku Corporation, Japan) and Fourier transform infrared spectroscopy (FTIR; Nicolet 380, Nicolet, USA) were employed to identify the crystal structure and the chemical bands of GO, RGO and GM composites. The molecular vibration modes and defects of samples were measured by Raman spectroscopy (Renishaw 2000 Confocal Raman Microprobe; Renishaw Instruments, England). The morphology and structure of the samples were investigated by field emission scanning electron microscopy (FESEM; Quanta 200F, FEI, Holand) and transmission electron microscopy (TEM; JEM-2010 HR, Jeol, Japan). Thermogravimetric measurements (TGA; SDT 2960, TA Instruments, American) were carried out to determine the weight percentage of Mn_3O_4 in GM composites of the RGO and GM composites.

2.4 Electrochemical measurements

The supercapacitor electrodes were prepared by pressing the mixture of as-prepared GM composites, acetylene black and polytetrafluoroethlene at a weight ratio of 8:1:1 onto the Ni foam and dried at 80 ^oC for 12 h. The electrodes were sliced into a 16.2 mm diameter wafer and packed into button-type supercapacitors using 5 M of NaOH aqueous solution as electrolyte. The electrochemical properties of packaged button cell were studied by cyclic voltammetry, galvanostatically charge/discharge measurements and AC impedance test. The Nyquist plots and CV curves were measured by an electrochemical work station (IM6) with the potential from 0 to 1.0 V at different scan rates. The cycle performance and the charge/discharge efficiency were tested by a LAND battery tester (CT2001A, Wuhan LAND Corporation, China) under the various current densities of charge/discharge. Meanwhile, RGO and pure Mn_3O_4 electrodes were also prepared and tested under the same condition for comparison.

3. Results and discussion

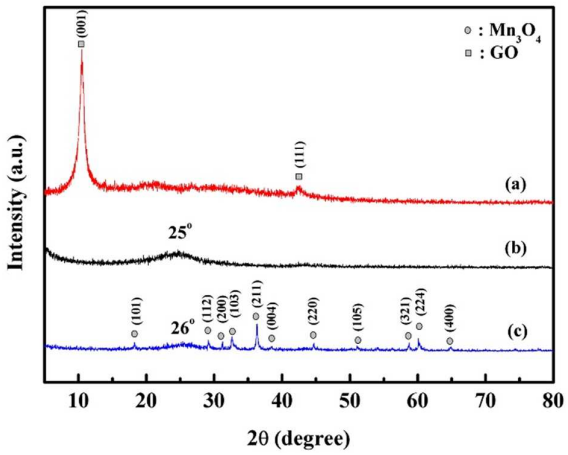

Fig. 1 XRD patterns of GO (a), RGO (b) and GM composites (c).

Fig. 1 shows the XRD patterns of GO, RGO and GM composites. As shown in Fig.1a, the diffraction peaks at 10.46° and 42.6° correspond to the (001) and (111) reflection of GO, indicating that graphite had been fully oxidized[24]. The interlayer spacing of GO was 0.87 nm, which was much larger than that of pristine graphite (0.34 nm) due to the introduction of oxygen-containing functional groups on the graphite sheets[22]. After microwave radiation treatment of GO, the (001) peak disappeared, while a new peak emerged at 25°, as shown in Fig. 1b. The peak with weaker intensity and wider shape corresponded to the disorderly stack and amorphous structure of RGO, resulting from the decomposition of oxygen-containing functional groups during the reduction of GO[23]. Fig. 1c shows the XRD pattern of GM composites. All diffraction peaks can be indexed to typical Hausmannite Mn_3O_4 (JCPDS card No. 24-0734). In addition, the peak of RGO at 25° was shifted to around 26 °, indicating that the residual oxygen-containing functional groups were further decomposed simultaneously during the final microwave irradiation.

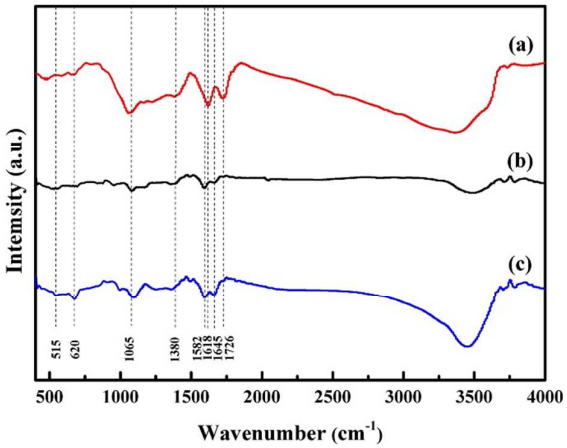

Fig. 2 FTIR spectra of GO (a), RGO (b) and GM composites (c).

FTIR spectroscopy was used to analysis the existence of oxygen-containing functional groups and their changes after microwave radiation treatment. Fig. 2 shows the FTIR spectra of GO, RGO and GM composites, respectively. As shown in Fig. 2a, a broad and intense absorption band appeared in the range of 3000-3700 cm^{-1} derived from the streching vibration of -OH. Two typical peaks at 1726 and 1618 cm^{-1} can be attributed to the stretching vibration of C=O in carboxy and the deformation vibration absorption peak of water molecules, respectively. Another two weak peaks at 1380 and 1065 cm^{-1} corresponded to C-O and the vibration adsorption peak of C-O-C, respectively[23]. Compared with GO, the intensity of all absorption peaks related to oxygen-containing functional groups in RGO (Fig. 2b) obviously decreased. The peaks at 1618 and 1726 cm^{-1} were almost disappeared, but the peaks at 1065, 1380 and 3364 cm^{-1} still existed, indicating that part of oxygen-containing functional groups were decomposed during microwave irradiation. Furthermore, a new absorption peak located at 1582 cm^{-1}, corresponding to the aromatic skeletal of C=C stretching vibration, was observed. The result further demonstrated the reduction of GO[25]. A new band at 1645 cm^{-1} originated from the O-H bending vibration of absorbed water molecules. For the GM composites, the absorption peaks at 1065, 1380, 1618, 1645 and 3364 cm^{-1} corresponded to RGO (Fig. 2c). Two extra broad absorption peaks at 515 and 620 cm^{-1} were associated with the coupling mode between octahedral sites and Mn-O stretching modes of tetrahedral[22]. The FTIR results further confirmed the reduction of GO and the formation of Mn_3O_4.

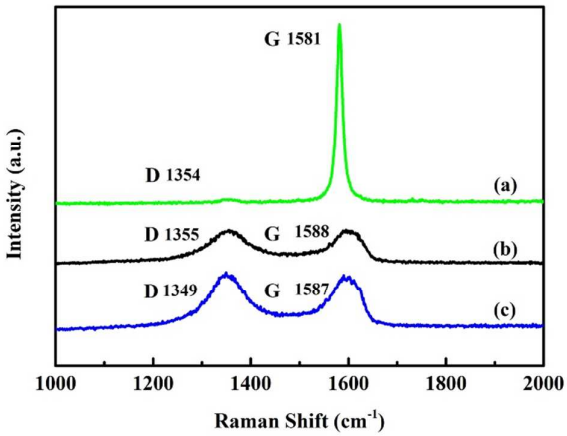

Fig. 3 The Raman spectra of graphite (a), RGO (b) and GM composites (c).

Raman spectroscopy is a powerful non-destructive technique to gain information of the ordered and disordered crystal structures of the samples. Fig. 3 shows the Raman spectra of natural graphite, RGO and GM composites. As shown in Fig. 3a, the natural graphite exhibits two Raman bands. The strong G band at 1581 cm^{-1} corresponded to the first-order scattering of E_{2g} mode, while the weak D band at 1354 cm^{-1} corresponded to graphite edges[26]. For the RGO and GM composites, two strong Raman peaks for G band and D band were also observed respectively, as shown in Fig. 3b and c. The ratio of the intensity of D and G band (I_D/I_G) for RGO was 0.96, which was dramatically higher than that of natural graphite (0.03), indicating much defects and high disorder in RGO resulted from the oxygen-containing defects due to the fiercely oxidation[27]. After hydrothermal treatment and microwave irradiation, the I_D/I_G of GM composites was increased to 1.12, indicating that more defects and disorder existed in GM composites than RGO due to the presence of Mn_3O_4 crystallites on graphene sheets.

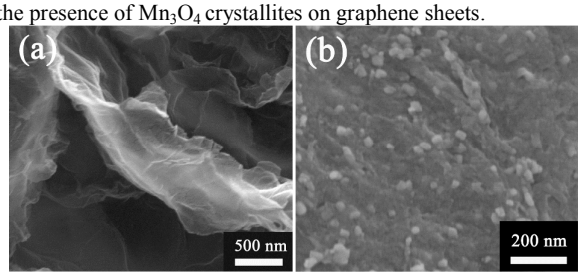

Fig. 4 FE-SEM images of RGO (a) and GM composites (b).

The surface morphologies of RGO and GM composites were studied by FE-SEM. RGO was crumpled into a curly and wavy sheet, and a few layers of RGO were stacked with each other, as shown in Fig. 4a. In the case of GM composites, the Mn_3O_4

nanoparticles were uniformly distributed on the surface of the RGO sheets (Fig. 4b). Further observation indicated that no stacking of graphene in the composites occurred, leading to a larger available surface area for energy storage.

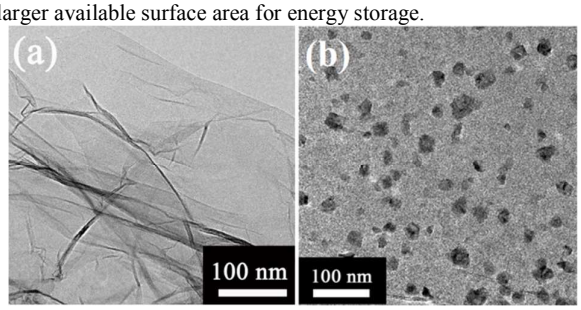

Fig. 5 TEM images of RGO (a) and GM composites (b).

Fig. 5 shows the TEM images of RGO and GM composites. As shown in Fig. 5a, RGO was transparent and a few layers of RGO were stacked with each other, which was consistent with the FE-SEM characterization. We can also observe in Fig. 5b that Mn_3O_4 nanoparticles with sizes of 20-50 nm were uniformly distributed on the transparent RGO sheets.

TGA measurements were employed to investigate the weight percentage of Mn_3O_4 in GM composites of RGO and the graphene in GM composites, as shown in Fig. 6. All samples were heated in a temperature range of 30-800 ^oC with a ramp rate of 20 ^oC min^{-1} in air. The weight loss of ca. 2.4% below 100 ^oC was due to the evaporation of the absorbed moisture. For the RGO, the weight loss was reached to 100% when the temperature reached to 800 ^oC, indicating that the RGO was completely burn off in air at 800 ^oC. For the GM composite, there was a weight loss of 65.7% at the temperature range of 100-800 ^oC, which can be attributed to the combustion of the grephene in the composites. Therefore, the content of Mn_3O_4 in GM composites was ~32.7 wt% (31.9%:97.6%).

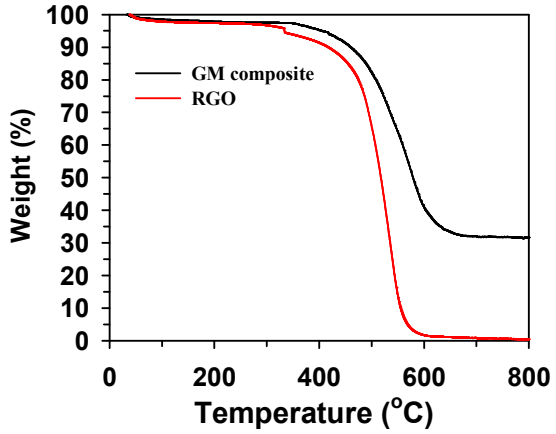

Fig. 6 TGA curves of RGO (a) and GM composites (b).

The as-prepared samples were fabricated into supercapacitor electrodes and tested by cyclic voltammetry measurement (CV) in a two-electrode symmetrical cell. The CV curves of the electrodes at a scan rate of 10 mV s^{-1} in the voltage range of 0-1.0 V using 5 M of NaOH aqueous solution as electrolyte was shown in Fig. 7a. The CV curves of RGO and GM composite were both near-rectangular and symmetric, indicating that they both possessed a perfect capacitive behavior and electrochemical performance. For the pure Mn_3O_4, a distorted CV curve was observed, which was probably caused by the poor electrical conductivity of pure Mn_3O_4. In addition, it is clearly seen that the CV loop of GM composite is much larger than those of RGO and Mn_3O_4. Fig. 7b shows the CV curves of GM measured at scan varying from 10 to 100 mV s^{-1}, which are also near-rectangular and symmetric, indicating that the GM exhibits good charge and discharge reversibility.

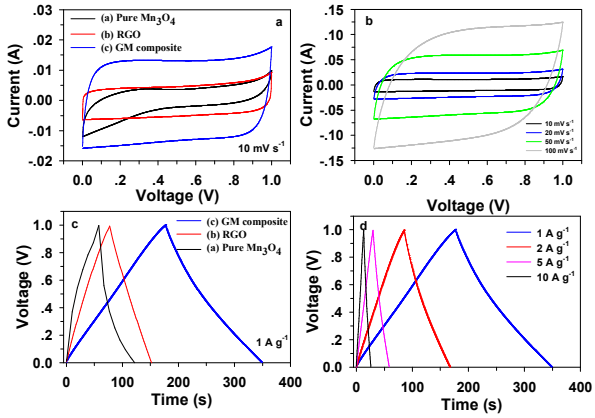

Fig. 7 The cyclic voltammograms of pure Mn_3O_4, RGO and GM composites at the scan rates of 10 mV s^{-1} (a), the cyclic voltammograms of GM composites measured at a scan rate varied from 10 to 100 mV s^{-1} (b), the charge/discharge curves of pure Mn_3O_4, RGO and GM composites electrodes at a current density of 1 A g^{-1} (c) and the charge/discharge curves of GM composites at the different current densities (d).

Fig. 7c shows the galvanostatic charge/discharge curves of pure Mn_3O_4, RGO and GM composites electrodes between 0 V and 1.0 V at a current density of 1 A g^{-1}. And the galvanostatic charge/discharge curves at different current densities as shown in Fig. 7d. The curves in the total range of 0-1.0 V were linear and symmetrical, indicating a good capacitive behavior. In the galvanostatically charge/discharge measurement, the specific capacitance of single electrode should be twice the supercapacitor in that the inner circuit of supercapacitor is equal to the series connection of two capacitors. the specific capacitance of single electrode (C_{single}) was calculated according to the following *Eq.* 1[23]:

$$C_{\text{single}} = 2 \cdot \frac{c}{m} = 2 \cdot \frac{\Delta Q}{m \cdot \Delta U} = 2 \cdot \frac{\Delta Q}{m \cdot \Delta t} \cdot \frac{\Delta t}{\Delta U} = 2 \cdot \frac{I \cdot \Delta t}{m \cdot \Delta U} \quad (1)$$

Where I (A) is the discharge current, Δt (s) is the discharging time, ΔU (V) represents the potential drop during discharge process, m (g) is the mass of the active materials in each electrode. The specific capacitance of RGO, pure Mn_3O_4 and GM composites electrodes at the current density of 1 A g^{-1} were 156.2, 128.6 and 344.8 F g^{-1}, respectively. Obviously, the GM composites exhibit the highest specific capacitance among them.

Fig. 8a shows the specific capacitance of samples at different current density. When the current density increased to 10 A g^{-1}, the specific capacitance of GM composites still kept at a high value of 258.1 F g^{-1} (~74.9% capacitance retention), which is far

larger than those of the RGO (115.0 F g^{-1}, ~73.6% capacitance retention) and pure Mn_3O_4 (29.5 F g^{-1}, ~22.9% capacitance retention). The result indicated that GM composites had a more excellent rate performance than pure Mn_3O_4. The enhanced capacitance and the excellent rate performance of GM composites were mainly attributed to the synergistic effect of the graphene and Mn_3O_4 nanoparticles. Firstly, uniform distribution of Mn_3O_4 nanoparticles on graphene sheets can eliminate restacking and agglomeration of graphene, and offer a high active surface for taking a full advantage of Mn_3O_4-based pseudocapacitance and graphene-based electric double-layer capacitance. Secondly, graphene with high electrical conductivity can serve as the electron superhighway, which facilitate a rapid and efficient charge transport, thus to improve the electronic conductivity of the overall system. Thirdly, the graphene can inhibit the aggregation of the Mn_3O_4 nanoparticles, thus to preserve the high-surface-area interface between the Mn_3O_4 nanoparticles and electrolytes.

Table1 Summary of electrochemical performance reported in literatures for Mn_3O_4/graphene composites as a supercapacitor electrode material in recent years.

Preparation method	Electrolyte	Measurement protocol	Maximun capacitance	Capacitance retention after cycle test	Ref（year）
Ultrasound assisted	1 M Na_2SO_4 6 M KOH	5 mV/s	175 F /g 256 F /g	_____	[19] 2010
Solvothermal	1 M Na_2SO_4	1 A/g	115 F /g	100% after 10000 cycles	[20] 2012
Microwave-assisted	0.5 M Na_2SO_4	25 mV/s	193 F /g	_____	[30] 2012
Solvothermal	1 M Na_2SO4	1 A/g	147 F /g	95% after 500 cycles	[21] 2012
Solvothermal	1 M Na_2SO_4	5 mV/s	225 F /g	82.1% after 900 cycles	[22] 2013
Solvothermal	0.5 M Na_2SO_4 5 mM $NaNCO_3$	1 A/g	205.5 F /g	98.7% after 2000 cycles	[31] 2013
Solvothermal	1 M Na_2SO4	0.1 A/g	171 F /g	92.9% after 50 cycles	[32] 2013
Dielectric barrier discharge (DBD) plasma-assisted	Saturated K_2SO_4	50 mA/g	260 F/g	92% after 800 cycles	[33] 2013
Chemical decomposition	1 M Na_2SO_4	0.5 A/g	131 F /g	99% after 500 cycles	[34] 2014
Combined modified Hummers	Saturated K_2SO_4	50 mA/g	260 F /g	94% after 1000 cycyles	[35] 2014
Ultrasound assisted	1 M Na_2SO_4	0.5mA/cm^2	312 F /g	76% after 1000 cycles	[36] 2015
Microwave-assisted	5 M NaOH	1 A/g	344.8 F /g	99.2% after 5000 cycles	This work

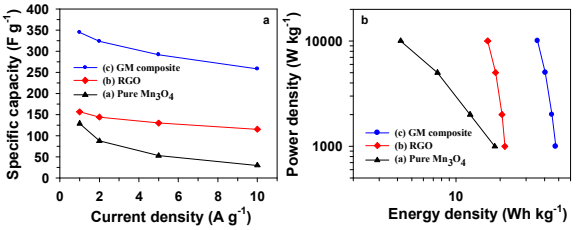

Fig. 8 Effects of current density on the specific capacitance of electrodes (a), and Ragone plots (b) of the supercapacitors based on pure Mn_3O_4, RGO and GM composites.

Fig. 8b shows the Ragone plots of the supercapacitors based on the RGO, pure Mn_3O_4 and GM composites. The energy density (E) and specific power density (P) of electrodes were calculated according to *Eq.* 2[28] and *Eq.* 3[28]:

$$E = \frac{\frac{1}{2}C(\Delta U)^2}{3.6} \quad (2)$$

$$P = \frac{Q \cdot \Delta U}{2t} = \frac{E}{t} \quad (3)$$

Where C, Q, ΔU and t are indicating of the specific capacitance of single electrode (F g^{-1}), total charge delivered (C), the potential window of discharge (V) and discharge time (s), respectively. The energy density of RGO, pure Mn_3O_4 and GM composites at a power density of 1000 W kg^{-1} were calculated to be 21.7, 17.9 and 47.8 Wh kg^{-1}, respectively. It can be found that the energy density of the GM composites was far higher than that of RGO and pure Mn_3O_4 at every power density. With the increase of the power density, the energy density of supercapacitor based on GM composites exhibits a small decrease, but that of the supercapacitor based on pure Mn_3O_4 displays a sharp decrease, indicating that the GM composites-based supercapacitor had excellent power and energy performance.

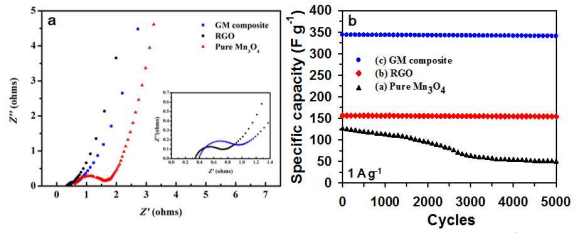

Fig. 9 EIS (a) and cycle performance measured at 1 A g^{-1} (b) for the supercapacitors based on pure Mn_3O_4, RGO and GM composites.

To investigate the transport characteristics of the charge carries in RGO, pure Mn_3O_4 and GM composites electrodes, the electrochemical impedance spectroscopy (EIS) of the supercapacitors was measured and the corresponding Nyquist plot was shown in Fig. 9a. Nyquist plot is a plot of the imaginary component (Z'') of the impedance against the real component (Z') reflecting the frequency response of electrode/electrolyte system. Apparently, a semicircle portion was observed at higher frequencies corresponding to the charge transfer limiting process. The slope portion of 45^o of the curve is called the Warburg resistance resulting from the frequency dependence of ions diffusion/transport in the electrolyte[6].

At higher frequencies, the relationship between Z' and Z'' can be described as *Eq.* 4, while at low frequencies, a straight line of the slope of 45^o can be obtained according to *Eq.* 5[29]:

$$\left[Z' - \left(\frac{R_{ESR} + R_r}{2}\right)\right]^2 + Z''^2 = \left(\frac{R_r}{2}\right)^2 \quad (4)$$

$$Z'' = Z' - R_{ESR} - R_r + 2\sigma^2 C_d \quad (5)$$

Where Z' is the real component, Z'' is the imaginary component, R_{ESR} (Ω) is the equivalent series resistance, R_r (Ω) is the reaction resistance, σ is the Warburg coefficient, and C_d (F) is the electric double layer capacitance of electrodes.

The Nyquist plot in Fig. 9a showed that equivalent series resistance (ESR) of the RGO, pure and GM composite systems were 0.33, 0.38 and 0.63 Ω, respectively, illustrating that the combination of high electrical conductive graphene with Mn_3O_4 resulted in a good conductivity of the overall system. Thisbehavior was attributed to the good conductivity of graphene matrix and the excellent contact between the graphene and Mn_3O_4 nanoparticles. The almost straight line of the slope of 45^o in the low-frequency region and the low R_{ESR} for GM composite system demonstrated that the electrodes based on GM composite can be used as ideal capacitors.

Cycling stability, one of most important requirements in practical application, was investigated in the range of 0-1 V at 1 A g^{-1} in 5 M of NaOH aqueous solution. Fig. 9b presents the cycling performance of RGO, pure Mn_3O_4 and GM composites with cycle times over 5000. It is found that the specific capacitance of pure Mn_3O_4 electrodes retained only about 39.2% after 5000 cycles. However, the curves of RGO and GM composites were almost smooth horizontal lines, showing an excellent cycle performance. The specific capacitance of GM composites electrodes slightly decreased from 344.8 to 342.1 F g^{-1}, retaining about 99.2% of initial capacitance after 5000 cycles. Compared with pure Mn_3O_4, the excellent cycling stability of GM composites was attributed to the excellent interconnection of Mn_3O_4 nanoparticles at the surface and interior of the electrodes. The uniform dispersion of Mn_3O_4 nanoparticles on the graphene sheets and the large distance between neighboring graphene sheets provided enough space to buffer the volume change of Mn_3O_4 nanoparticles during charge/discharge redox reaction. Table 1 summarizes electrochemical performance reported in literature for Mn_3O_4/graphene composites as a supercapacitor electrode material. It is clear that our as-papered electrodes are superior to those of most recent counterparts in performance.

4. Conclusion

GM composites have been successfully fabricated through microwave-assisted in-situ hydrothermal synthesis of Mn_3O_4 nanoparticles on the RGO. The supercapacitors based on GM composites electrodes showed excellent electrochemical performance. With 5 M of NaOH as the electrolyte, supercapacitor electrodes based on GM composites material showed a specific capacitance as high as 344.8 F g^{-1} at the current density of 1 A g^{-1} in the voltage range of 0-1.0 V and a high energy density up to 47.8 Wh kg^{-1} at the power density of 1000 W kg^{-1}. Furthermore, the GM composites exhibited good cycling stability with little decay after 5000 cycles. The supercapacitor electrodes based on GM composites with excellent electrochemical properties and stability are expected to find widely promising applications in high-performance supercapacitors.

Acknowledgements

This work is supported by the link project of the National Natural Science Foundation of China and Guangdong Province (No. U1401246), the National Natural Science Foundation of China (Grant No. 51276044), and the Natural Science Foundation of Guangdong Province of China (No. 2014A030310382).

References

1 J. R. Miller, P. Simon, *Science*, 2008, **321**, 651-652.
2 M. Noked, A. Soffer, D. Aurbach, *J. Solid State Electrochem.*, 2011, **15**, 1563-1578.
3 T. Brezesinski, J. Wang, S. H. Tolbert, B. Dunn, *Nat. Mater.*, 2010, **9**, 146-151.
4 H. Wang, Z. Liu, X. Chen, P. Han, S. Dong, G. Cui, *J. Solid State Electrochem.*, 2011, **15**, 1179-1184.
5 R. H. Baughman, A. A. Zakhidov, W. A. de Heer, *Science*, 2002, **297**, 787-792.
6 M. D. Stoller, S. Park, Y. Zhu, J. An, R. S. Ruoff, *Nano Lett.*, 2008, **8**, 3498-3502.
7 A. G. Pandolfo, A. F. Hollenkamp, *J. Power Sources*, 2006, **157**, 11-27.
8 S. Sarangapani, B. Tilak, C. P. Chen, *J. Electrochem. Soc.*, 1996, **143**, 3791-3799.
9 J. Li, X. Wang, Q. Huang, S. Gamboa, P. Sebastian, *J. Power Sources*, 2006, **158**, 784-788.
10 X. Cao, Y. Shi, W. Shi, G. Lu, X. Huang, Q. Yan, Q. Zhang, H. Zhang, Small, 2011, **7**, 3163-3168.
11 G. Yu, L. Hu, N. Liu, H.Wang, M. Vosgureitchian, Y. Yang, Y. Cui, Z. Bao, Nano Lett., 2011, **11**, 4438-4442.
12 B. Jiang, Y. Liu, Z. Wu, *J. Hazard. Mater.*, 2009, **162**, 1249-

1254.
13 S.-B. Ma, K.-W. Nam, W.-S. Yoon, S.-M. Bak, X.-Q. Yang, B.-W. Cho, K.-B. Kim, *Electrochem. Commun.*, 2009, **11**, 1575-1578.
14 X. Q. Yu, Y. He, J. P. Sun, K. Tang, H. Li, L. Q. Chen, X. J. Huang, *Electrochem. Commun.*, 2009, **11**, 791-794.
15 D. Bélanger, L. Brousse, J. W. Long, *The Electrochemical Society Interface*, 2008, **17**, 49.
16 S. V. Morozov, K. S. Novoselov, M. I. Katsnelson, F. Schedin, D. C. Elias, J. A. Jaszczak, A. K. Geim, *Phys. Rev. Lett.*, 2008, **100**.
17 A. A. Balandin, S. Ghosh, W. Bao, I. Calizo, D. Teweldebrhan, F. Miao, C. N. Lau, *Nano Lett.*, 2008, **8**, 902-907.
18 S. Stankovich, D. A. Dikin, G. H. B. Dommett, K. M. Kohlhaas, E. J. Zimney, E. A. Stach, R. D. Piner, S. T. Nguyen, R. S. Ruoff, *Nature*, 2006, **442**, 282-286.
19 B. Wang, J. Park, C. Wang, H. Ahn, G. Wang, *Electrochim. Acta*, 2010, **55**, 6812-6817.
20 J. W. Lee, A. S. Hall, J.-D. Kim, T. E. Mallouk, *Chem. Mater.*, 2012, **24**, 1158-1164.
21 X. Zhang, X. Sun, Y. Chen, D. Zhang, Y. Ma, *Mater. Lett.*, 2012, **68**, 336-339.
22 Y. Wu, S. Liu, H. Wang, X. Wang, X. Zhang, G. Jin, *Electrochim. Acta*, 2013, **90**, 210-218.
23 J. Ye, H. Zhang, Y. Chen, Z. Cheng, L. Hu, Q. Ran, *J. Power Sources*, 2012, **212**, 105-110.
24 B. Zhao, J. Song, P. Liu, W. Xu, T. Fang, Z. Jiao, H. Zhang, Y. Jiang, *J. Mater. Chem.*, 2011, **21**, 18792-18798.
25 Z. Wu, W. Ren, L. Gao, J. Zhao, Z. Chen, B. Liu, D. Tang, B. Yu, C. Jiang, H.-M. Cheng, *ACS Nano*, 2009, **3**, 411-417.
26 F. Tuinstra, J. L. Koenig, *J. Chem. Phys.*, 1970, **53**, 1126-1130.
27 A. Ferrari, J. Meyer, V. Scardaci, C. Casiraghi, M. Lazzeri, F. Mauri, S. Piscanec, D. Jiang, K. Novoselov, S. Roth, *Phys. rev. Lett.*, 2006, **97**, 187401.
28 J. Yan, Z. Fan, T. Wei, J. Cheng, B. Shao, K. W, L. Song, M. Zhang, *J. Power Sources*, 2009, **194**, 1202-1207.
29 Z. Huang, H. Zhang, Y. Chen, W. Wang, Y. Chen, Y. Zhong, *Electrochim. Acta*, 2013, **108**, 421-428.
30 C. Liu, K. Chang, C. Hu, W. Wen, J. Power Sources, 2012, **217**,184-192.
31 S. Yang, X. Song, P. Zhang, L. Gao, J. Mater. Chem., 2013,**1**,14162.
32 Y. Fan , X. Zhang , Y. Liu , Q. Cai, J. Zhang, Mater. Lett. , 2013,**95**,153-156.
33 J. Qu, F. Gao, Q. Zhou, Z. Wang, H. Hu, B. Li, W. Wan, X. Wang, J. Qiu, Nanoscale, 2013,**5**,2999-3005.
34 K. Subramani,D. Jeyakumara, M. Sathish, Phys. Chem. Chem. Phys., 2014,**16**, 4952-4961.
35 F. Gao, J. Qu , Z. Zhao , Q. Zhou , B. Li, J. Qiu, Carbon, 2014,**80**,640-650.
36 B.G.S. Raj, R.N.R. Ramprasad, A.M. Asiri, J.J. Wu, S. Anandan, Electrochim. Acta, 2015,**156**,27-137.